Electronic Supplementary Material (ESI) for Physical Chemistry Chemical Physics.

First-principles study of high spin rectification effect device based on Nitride MXene (Sc_2NO_2, Ti_2NO_2)

Pengwei Gong[a], Xiaolin Zhang[a], Fangqi Liu[a], Sicong Zhu[a,*]

a The State Key Laboratory for Refractories and Metallurgy, Hubei Province Key Laboratory of Systems Science in Metallurgical Process, Collaborative Innovation Center for Advanced Steels, International Research Institute for Steel Technology, Wuhan University of Science and Technology, Wuhan 430081, China

Email: sczhu@wust.edu.cn (Sicong Zhu)

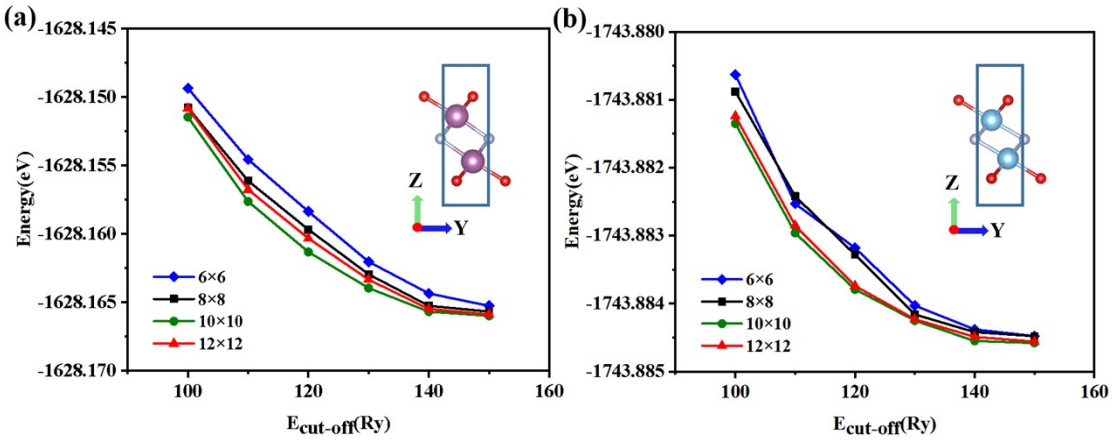

Fig. S1. The convergence test of k-point mesh with energy cutoff for (a) Sc_2NO_2 (b) Ti_2NO_2.

In order to reduce the manual errors associated with the experimental parameter settings, we first tested the convergence of the energy cut-off with the k-point mesh. As shown in Fig. S1(a), we can see that the energy value is lowest when the k-point mesh is chosen 10×10×1 for Sc_2NO_2, and the energy change is less than 0.0001 eV when the energy cutoff of the plane-wave basis is 150 Ry. Similarly, for Ti_2NO_2 Fig. S1(b), the lowest energy values are reached when the k-point mesh is chosen at 10×10×1, and the energy change is less than 0.0001 eV when the energy cutoff of the plane-wave basis reaches 140 Ry. In summary, we finally chose a k-point mesh of 10×10×1 with an energy cutoff of 150 Ry as the calculation parameter.

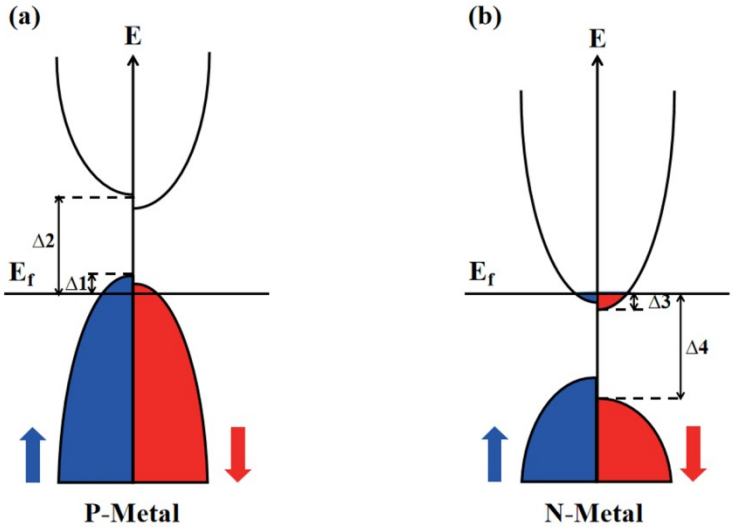

Fig. S2. The schematic diagram of band structure for (a) P-type magnetic metal and (b) N-type magnetic metal.

The schematic diagram of band structures for P-type magnetic metal and N-type magnetic metal is drawn in Fig. S2. For P-type magnetic metal, the distance from the conduction band minimum (CBM) to the Fermi level is greater than the distance from the valence band maximum (VBM) to the Fermi level ($\Delta 2 > \Delta 1$). However, for N-type magnetic metal, the distance from VBM to Fermi level is higher than that from CBM to Fermi level ($\Delta 4 > \Delta 3$). Compared with traditional magnetic materials, P-type magnetic metal (N-type magnetic metal) has not only discontinuous band distribution at the Fermi level but also greater electron transfer ability. Therefore, the properties of magnetic metal and magnetic semimetal can be obtained simultaneously through the regulation of the external electric field. Taking the characteristic of P-type magnetic metal and N-type magnetic metal, we can construct a spin diode with a high spin rectification effect.

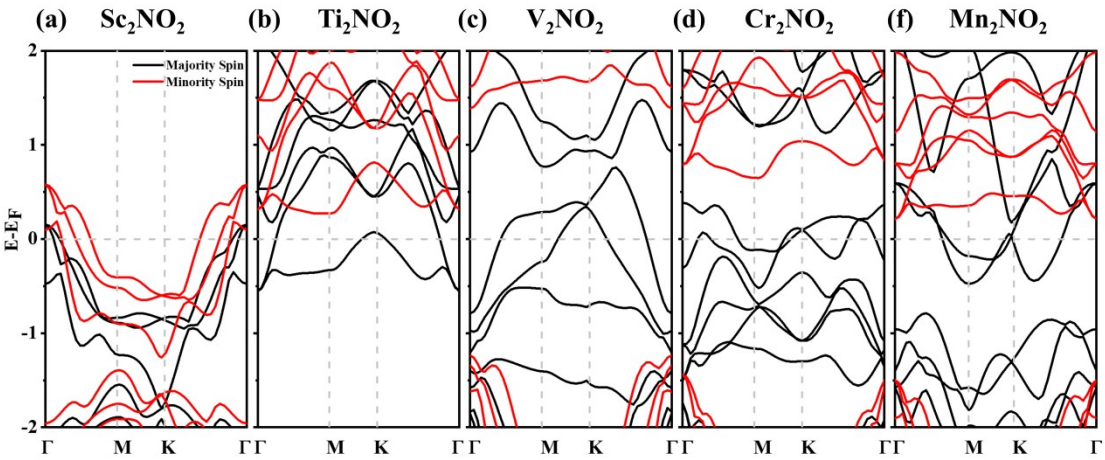

Fig. S3. (a)-(f) The band structure diagram of M_2NO_2(M=Sc, Ti, V, Cr, Mn), black lines and red lines represent the majority spin and minority spin respectively.

As shown in Fig. S3(a)-(f), the band structures of M_2NO_2(M=Sc, Ti, V, Cr, Mn) are drawn respectively. The path of the Brillouin zone is chosen as Γ→M→ K→Γ. In Fig. S3(a), for Sc_2NO_2, both majority spin and minority spin bands pass through the Fermi level at the same time. The distance from the conduction band minimum (CBM) to the Fermi level for both spin states is much higher than the distance from the valence band maximum (VBM) to the Fermi level, which exhibits the properties of P-type metals. However, in Fig. S3(b), the bands of majority spin pass through the Fermi level, and the minority spin bands remain in the 0.2 V energy level region for Ti_2NO_2. Moreover, the distance between VBM and the Fermi level for two spin states is greater than the distance from CBM to the Fermi level, showing the characteristics of N-type half-metals. Besides, for V_2NO_2, Cr_2NO_2, and Mn_2NO_2 (Fig. S3(c)-(e)), only the majority-spin bands go through the Fermi level, so they all behave like half-metals.

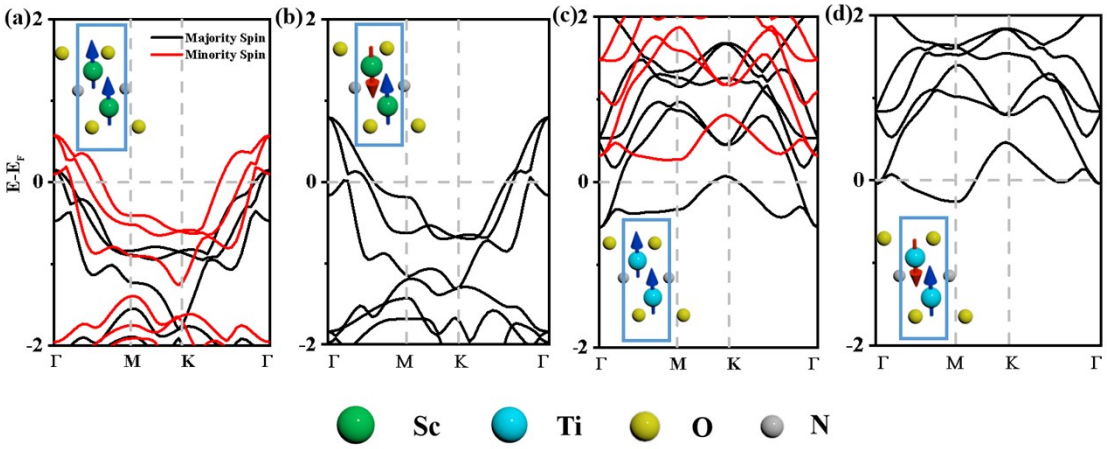

Fig. S4. The energy bands of the Sc_2NO_2 in (a) ferromagnetic state and (b) antiferromagnetic state. The energy bands of the Ti_2NO_2 in (c) ferromagnetic state and (d) antiferromagnetic state. The black and red lines indicate the majority and minority spin bands, respectively. Green, blue, yellow and grey spheres indicate Sc, Ti, O and N atoms, respectively.

As shown in Fig. S4, the band structures of the two Nitride MXene (Sc_2NO_2 and Ti_2NO_2) in the ferromagnetic and anti-ferromagnetic states are plotted. It can be seen that the majority spin bands overlap with the minority spin bands in the anti-ferromagnetic state, which implies the loss of magnetism.

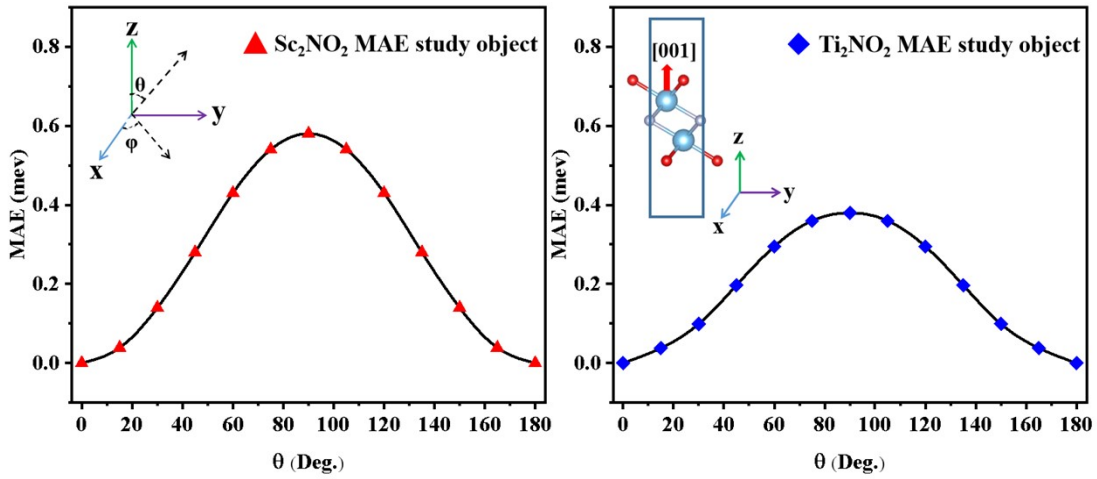

Fig. S5. Magnetic anisotropy energy varies with the polar angle (θ) for (a) Sc_2NO_2 (b) Ti_2NO_2.

The magnetic anisotropy energy (MAE) of two Nitride MXene (Sc_2NO_2 and Ti_2NO_2) varies with the θ are shown in Fig. S5. The MAE is defined as the energy difference between the two spin directions, and the highest value denoting the energy difference between θ = 0°and θ = 90°. The positive MAE value means that the energy in the spin direction of θ = 0°is lower than that in the direction of θ = 90°. Moreover, We also investigated the relationship between the variation of MAE with φ by fixing θ = 0°, 30°, 60°, 90°, 120°, 150°and 180°to change the φ (0°≦ φ≦ 180°). The results show that the energy does not vary with the increasing φ when θ is certain. The MAE exhibits a strong dependence on the polar angle (θ), and a much weaker dependence on the azimuthal angle (φ). So for Sc_2NO_2 and Ti_2NO_2, the easy axes of localized spin is found to be the [001] direction (along the Z axis).

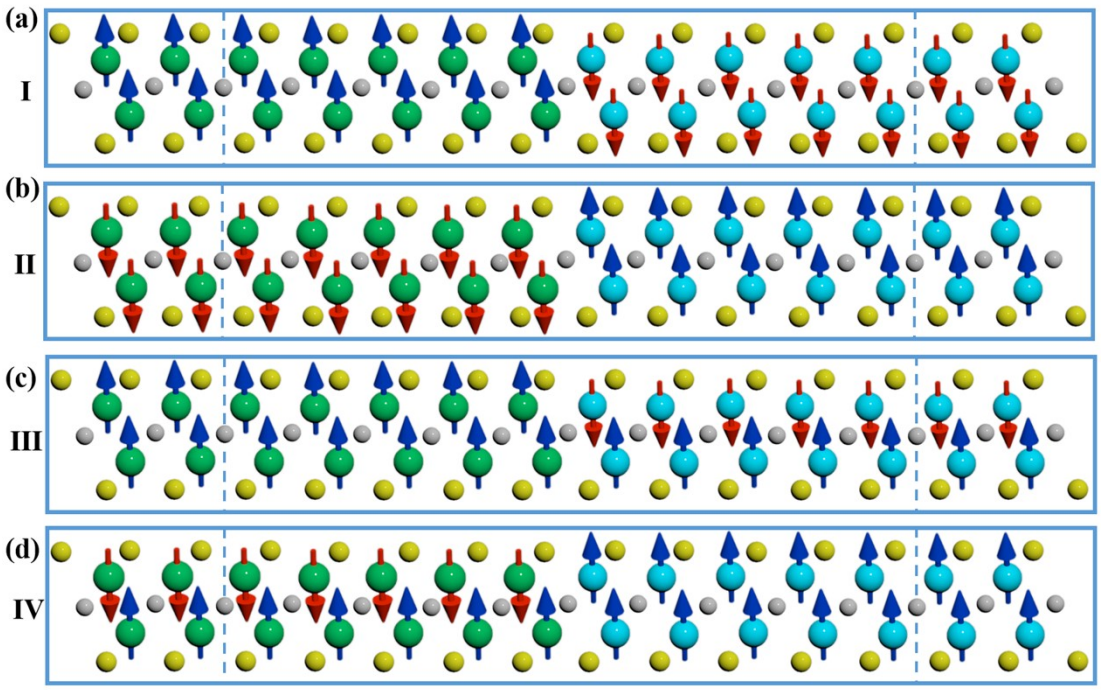

Fig. S6. Heterostructures with four different forms of magnetic coupling, (a) Device I is Sc_2NO_2 magnetised up with Ti_2NO_2 magnetised down. (b) Device II is Sc_2NO_2 magnetised down with Ti_2NO_2 magnetised up. (c) Device III is Sc_2NO_2 ferromagnetic state with Ti_2NO_2 antiferromagnetic state. (d) Device IV is Sc_2NO_2 antiferromagnetic state with Ti_2NO_2 ferromagnetic state.

We change the magnetic coupling style of the Sc_2NO_2/Ti_2NO_2 heterojunction. For the heterojunction, we keep the magnetisation direction of the P or N components respectively then adjust another component to the opposite magnetisation direction (Fig. S6 (a) and (b)). On the other hand, as shown in Fig. S6 (c) and (d), we maintain the ferromagnetic state of the P or N component respectively, while adjusting another component to the anti-ferromagnetic state.

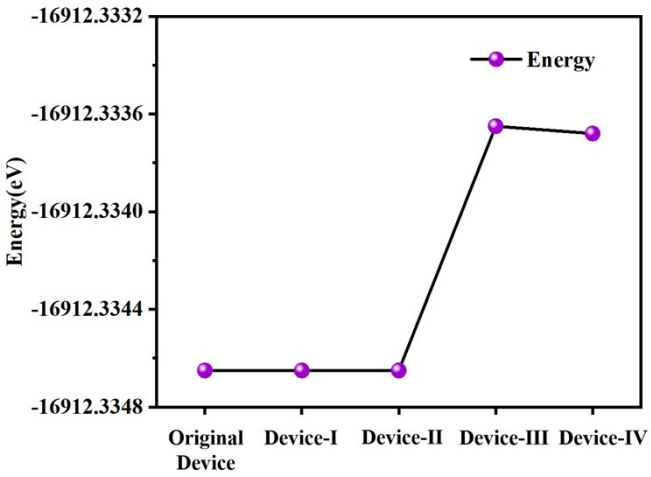

Fig. S7. The energy of parallel-state device (in the original paper) and four anti-parallel-state

devices (I, II, III, and IV).

In Fig. S7, we compare the energy of parallel-state device (in the original paper) and four anti-parallel-state devices (I, II, III, and IV). It can be seen that the parallel-state device and device I(II) have the lowest energy.

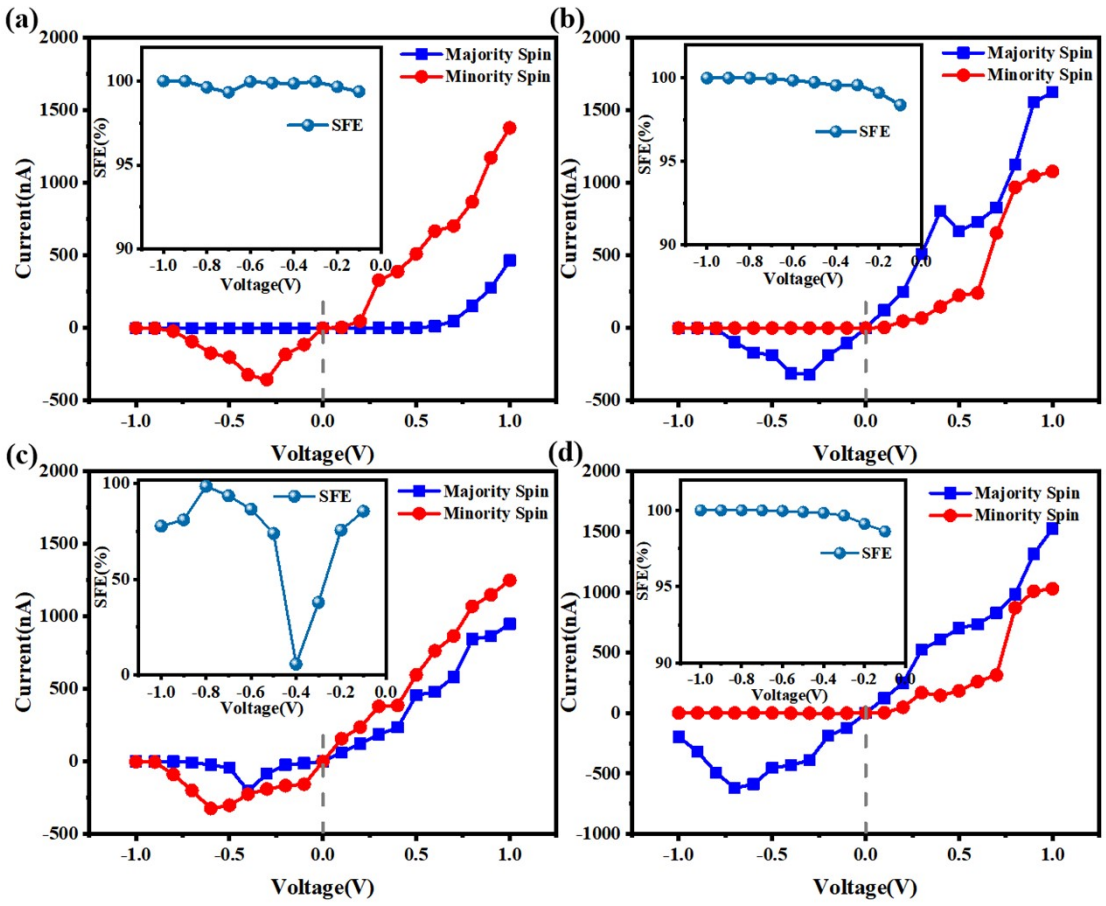

Fig. S8. The curves of spin currents with bias [-1,1] for devices I, II, III and IV, the inset picture is the corresponding spin filtering efficiencies.

The IV curves for four heterojunctions with different magnetic coupling states are shown in Fig. S8. In Fig. S8 (a), the minority spin current is much higher than the majority spin current, and the great spin filtering efficiency is still maintained under negative bias when the N component is changed to the opposite magnetisation direction. On the contrary, the majority spin current is higher than the minority spin current when the magnetisation direction of the P component is changed in Fig. S8 (b). And the spin filtration efficiency also close to 100% exists at the negative bias. In addition, when keeping the P or N component in the ferromagnetic state respectively and changing another component to the anti-ferromagnetic state, the I-V curves are shown in Fig. S8 (c) and (d). The current dominated by the minority spin when the N component in the anti-ferromagnetic state. And it has a greater impact on the spin

filtering efficiency. However, when the P component in the anti-ferromagnetic state, the current mainly dominated by the majority spin. These differences are mainly caused by the change in the band structure and magnetism of the P (N) components. In summary, changing the magnetic coupling style of the heterojunction will affect the spin current and spin rectification efficiency.

Acknowledgements

The author would like to thank the National Natural Science Foundation of China under Grants (No. 11704291 and No. 51875417), Hubei Province Key Laboratory of Systems Science in Metallurgical Process (Wuhan University of Science and Technology, No.Y202101) , Key Laboratory of Nanodevices and Applications, Suzhou Institute of Nano-Tech and Nano-Bionics, Chinese Academy of Sciences (No.21YZ03) and High-Performance Computing Center of Wuhan University of Science and Technology.